J. Plasma Physics (2001), *vol.* 66, *part* 5, *pp.* 315–336.
DOI: 10.1017/S0022377801001477 Printed in the United Kingdom

Cascade of parametric instabilities in ionospheric heating experiments

S. P. KUO

Department of Electrical Engineering, Polytechnic University, 901 Route 110, Farmingdale, NY 11735, USA

(Received 16 March 2001)

Abstract. Two secondary parametric instabilities providing cascade channels for the Langmuir sidebands of the oscillating two-stream instability (OTSI) and parametric decay instability (PDI), which are excited by O-mode high-frequency (HF) heating waves, are studied. The first one decays a Langmuir pump wave into a Langmuir sideband and an ion acoustic decay mode. Both resonant and nonresonant cascade processes are considered. Nonresonant cascade of Langmuir waves proceeds at the same location and is increasingly hampered by the frequency mismatch effect. Resonant cascade takes place in different resonant locations to minimize the frequency mismatch effect, but it has to overcome the severe propagation loss of the mother Langmuir wave in each cascade step. This process produces a narrow spectrum of frequency-downshifted (from the HP wave frequency) plasma waves. The second employs the lower-hybrid wave as the decay mode. Only the nonresonant cascade is of interest, because the propagation loss of the mother Langmuir wave in each resonant cascade step is far too severe. This is a three-dimensional coupling process, because the wavevectors of coupled three waves have to be matched in three-dimensional space, rather than matched in the conventional way on the plane of the pump wavevector and the geomagnetic field. A broad spectrum of frequency-downshifted plasma waves can be produced by this process in a narrow altitude range preferentially located near the matching heights of Langmuir sidebands of the OTSI and PDI.

1. Introduction

In the high-frequency (HF) heating and modification of the ionosphere, parametric instabilities provide effective channels to convert the ground-transmitted electromagnetic (EM) heating waves into electrostatic plasma waves of high and low frequencies. Many radar observations on plasma lines and ion lines (Carlson et al. 1972; Showen and Kim 1978; Hagfors et al. 1983; Stubbe et al. 1992; Westman et al. 1995; Lee et al. 1998, 1999) and ground measurements on stimulated electromagnetic emissions (SEEs) in ionospheric heating experiments have been understood in terms of the physical processes of various parametric instabilities. In midlatitude regions such as at Arecibo, Puerto Rico, the parametric instabilities are excited near the reflection height of the O-mode HF heating wave (Carlson et al. 1972), which is linearly polarized in the geomagnetic field direction. Hence, the sidebands excited by both the parametric decay instability (PDI) and the oscillating two-stream instability (OTSI) are Langmuir waves, which are excited most strongly

with propagation directions parallel to the geomagnetic field (Fejer and Kuo 1973; Perkins et al. 1974; Kuo et al. 1993; Kuo and Lee 1999). Some of these waves effectively detected by backscatter radars in heating experiments are termed 'HFPLs', which account only for those Langmuir waves having a wavenumber twice that of the probing radar signal and propagating in a direction parallel or antiparallel to the pointing direction of the radar.

Likewise, in high-latitude heating experiments, the PDI and OTSI are also expected to be excited by the O-mode HF heating wave near its reflection height, to produce Langmuir waves as the high-frequency sidebands of the instabilities. However, these instabilities have to compete with those occurring in the upper-hybrid resonance region located at a lower height, where the O-mode heating wave is still dominated by the field component of right-hand circular polarization. It has been shown that thermal parametric instabilities can be effectively excited in this height region. Sidebands of instabilities are upper-hybrid waves propagating nearly perpendicular to the geomagnetic field (Lee and Kuo 1983; Stenflo 1985, 1991; Stenflo and Shukla 1988; Leyser 1991; Huang and Kuo 1994; Zhou et al. 1994; Istomin and Leyser 1995; Kuo and Huang 1996; Kuo et al. 1997). Upper-hybrid waves were found to play a key role in the generation of 'stimulated electromagnetic emissions (SEEs)', observed in Tromsø heating experiments (Thide et al. 1982; Stubbe et al. 1982, 1984, 1994; Leyser et al. 1989; Stenflo 1990; Stubbe and Kopka 1990; Leyser 1994; Kuo 1997). Due to the field-aligned nature of upper-hybrid waves, these waves cannot be detected directly by EISCAT's UHF and VHF radar, and do not contribute to Tromsø's HFPLs.

Nevertheless, HFPLs have been detected by EISCAT's 933 MHz (UHF) and 244 MHz (VHF) radar during the Tromsø heating experiments (Hagfors et al. 1983; Stubbe et al. 1985, 1992; Westman et al. 1995; Stubbe 1996; Isham et al. 1999; Rietveld et al. 2000), except that the zero-offset frequency plasma line was detected only by the UHF radar, but not by the VHF radar (Stubbe et al. 1992). This suggested that the OTSI, which has a higher threshold than the PDI, were suppressed by instabilities draining heating-wave energy in the upper-hybrid resonance region. It was then shown by Kuo et al. (1997) that the zero-offset frequency plasma line detected by the UHF radar was excited by upper-hybrid waves generated by the HF heating wave in the upper-hybrid resonance region. The excitation process is also an OTSI, except that the pump wave of the instability is the upper-hybrid wave rather than the HF heating wave. The wavelengths of the excited Langmuir waves have an upper bound. This explains why the VHF radar did not detect the zero-offset frequency plasma line.

Moreover, the large difference in the magnetic dip angle could also cause the spectral features of frequency-downshifted HEPLs observed in Arecibo heating experiments different from Tromsø's. Usually, frequency-downshifted HEPLs observed in heating experiments have narrow spectra. In Tromsø, the results of early experiments, conducted by progressive increase of heating power within the range of available powers ($\sim$240 MW ERP), indicated that the number of cascade lines in HFPLs recorded by EISCAT's UHF and VHF radar was limited to two, independent of input power (Stubbe et al. 1992; Stubbe 1996). This was also the case in the later experiment as heating power was increased to 270 MW ERP (Rietveld et al. 2000). As heating power was further increased to 1200 MW ERP, up to five cascade lines in Tromsø's HFPLs were observed for the first time by Westman et al. (1995). Although the O-mode HF heating-wave electric field was expected to in-

crease considerably by a swelling factor, the most intense cascade lines in Tromsø's HFPLs were found to originate from the matching height of the PDI line in HFPLs (Rietveld et al. 2000), which is located at a lower altitude for UHF radar-detected lines than that for VHF radar-detected lines (Stubbe 1996). On the contrary, with improved spatial resolution of radar detection, Arecibo's HFPLs detected recently from a narrow altitude region were found occasionally to have a broad frequency-downshifted spectrum with a bandwidth as large as 50 kHz. This spectral feature is also characteristically different from the broad spectrum detected in Tromsø heating experiments, which is frequency-upshifted and much wider, and originates from the region above the HF reflection height (Isham et al. 1990; Mishin et al. 1997; Kuo et al. 1998). The physical process responsible for the generation of such a broad frequency-downshifted spectrum in Arecibo's HFPLs has been a subject of considerable interest.

In the present work, the PDI and OTSI and the subsequent cascades via two secondary parametric instability processes are analyzed systematically to explore the underlying mechanism that impedes the cascade process, and the mechanism that is responsible for the generation of a broad spectrum of frequency-downshifted HFPLs originating from a narrow altitude region. The Langmuir waves generated by the OTSI and PDI directly and indirectly can also cascade through alternative decay channels (Kaysmov et al. 1985). They will also introduce a significant perturbation to the background plasma, which, in turn, can further modify the spectral distribution in time. Such a self-consistent analysis (Kuo et al. 1987, 1990) leading to features such as the plasma line overshoot phenomena observed in HF heating experiments (Showen and Behnke 1978; Showen and Kim 1978) is, however, not included in the present work.

It is also worth pointing out that one- and two-dimensional models based on driven and damped Zakharov-type equations (Zakharov 1972; Zakharov et al. 1972) have also been introduced to study wave–wave interactions in heating experiments. The simulation effort represents a different approach to address different wave–wave interaction problems in ionospheric heating experiments. The differences between parametric couplings considered in the present work and the numerical simulations can be summarized as follows. The phase relationships among coupled waves are critical to the parametric coupling, while the constraints of the phase relationships have been significantly loosened in the formulation of the Zakharov equations. One of the cascade process considered in the present work has to be a three-dimensional process, which certainly cannot be simulated by one- or two-dimensional models. One of the significant results of the present work is to rigorously prove that the parametric instabilities (PDI and OTSI) and the subsequent cascades considered in the present work favor excitation in regions near the matching heights of those instabilities, rather than the reflection height of the O-mode HF pump. On the other hand, the approximations used in the derivation of Zakharov-type equations for simulating ionospheric heating experiments are based on the assumption that wave–wave couplings occur in the region near the HF reflection height. The approximations are not justifiable in the matching height region, because phase variations can no longer be neglected.

The coupled mode equations for parametric excitation of Langmuir waves are formulated in Sec. 2. The PDI and OTSI are first reviewed in Secs 3 and 4, respectively. In Sec. 5, cascades of PDI- and OTSI-excited Langmuir waves through the ion acoustic wave are studied. In Sec. 6, a three-dimensional cascade process

based on the decay of an obliquely propagating Langmuir pump wave into another obliquely propagating Langmuir wave (sideband) and a lower-hybrid decay mode is analyzed. In this parametric coupling, the wavevectors of three waves are matched in three-dimensional space, rather than matched in the conventional way on the plane of the pump wavevector and the geomagnetic field. The results are discussed in Sec. 7.

2. Coupled mode equations for parametric instabilities

Parametric excitation of Langmuir waves $\phi(\omega, \mathbf{k})$ and low-frequency plasma waves $n_s(\omega_s, k_s)$ by electromagnetic or Langmuir pump waves $\mathbf{E}_p(\omega_0, \mathbf{k}_p)$ are considered, where $\mathbf{E}_p, \phi$, and n_s denote electric field of a pump wave, the electrostatic potential of a Langmuir sideband, and the density perturbation of a low-frequency decay mode, respectively. Langmuir waves can have large oblique propagation angles (with respect to the background magnetic field $\mathbf{B}_0 = \hat{\mathbf{z}}B_0$), and low-frequency plasma waves include ion acoustic waves, purely growing modes, and lower-hybrid waves.

The coupled mode equation for the Langmuir sideband is derived from the electron continuity and momentum equations, and Poisson's equation:

$$\partial_t n_e + \boldsymbol{\nabla} \cdot (n_e \mathbf{v}_e) = 0, \tag{1}$$

$$(\partial_t + \nu_e) n_e \mathbf{v}_e + \boldsymbol{\Omega}_e n_e \mathbf{v}_e \times \hat{\mathbf{z}} = -\boldsymbol{\nabla} \cdot (n_e \mathbf{v}_e \mathbf{v}_e) - 3v_{te}^2 \boldsymbol{\nabla} \delta n_e - \frac{e}{m_e} n_e \mathbf{E}, \tag{2}$$

$$\nabla^2 \phi = 4\pi e \delta n_e. \tag{3}$$

where $n_e = n_0 + \delta n_e + n_s; n_0$ and δn_e are the unperturbed plasma density and electron density perturbation associated with Langmuir waves, respectively; the electron collision frequency ν_e includes a phenomenological term $\sim (\frac{1}{2}\pi)^{1/2}(\omega_0^4/k_z^2 k)$ $\exp(-\omega_0^2/2k_z^2 v_{te}^2)$ to account for the electron Landau-damping effect, $\boldsymbol{\Omega}_e = eB_0/m_e c$ is the electron cyclotron frequency; $v_{te} = (T_e/m)^{1/2}$ is the electron thermal speed; $\mathbf{E} = \mathbf{E}_P + \mathbf{E}_L$ and $\mathbf{E}_L = -\boldsymbol{\nabla}\phi$; and the relationship $\boldsymbol{\nabla} P_e = 3T_e \boldsymbol{\nabla} \delta n_e$ is used.

With the aid of (3) and the two orthogonal components of (2),

$$(\partial_t + \nu_e) n_e \mathbf{v}_e \times \hat{\mathbf{z}} = \boldsymbol{\Omega}_e n_e \mathbf{v}_{e\perp} - \boldsymbol{\nabla} \cdot (n_e \mathbf{v}_e \mathbf{v}_e) \times \hat{\mathbf{z}} - \left(3v_{te}^2 \boldsymbol{\nabla} \delta n_e + \frac{e}{m_e} n_e \mathbf{E}\right) \times \hat{\mathbf{z}} \tag{4}$$

and

$$(\partial_t + \nu_e) n_e \mathbf{v}_{ez} = -\boldsymbol{\nabla} \cdot (n_e \mathbf{v}_e \mathbf{v}_{ez}) - \left(3v_{te}^2 \boldsymbol{\nabla}_z \delta n_e + \frac{e}{m_e} n_e \mathbf{E}_z\right), \tag{5}$$

the three orthogonal components of (2) are combined into a single scalar equation:

$$\begin{aligned}
&(\partial_t + \nu_e)[(\partial_t + \nu_e)^2 + \boldsymbol{\Omega}_e^2] \boldsymbol{\nabla} \cdot (n_e \mathbf{v}_e) \\
&\quad = -[(\partial_t + \nu_e)^2 + \boldsymbol{\Omega}_e^2](3v_{te}^2 \nabla^2 \delta n_e - \omega_p^2 \delta n_e) + \boldsymbol{\Omega}_e^2 \nabla_\perp^2 \left(3v_{te}^2 \delta n_e - \frac{e}{m_e} n_0 \phi\right) \\
&\qquad -\{\boldsymbol{\Omega}_e^2 \partial_z n_e v_e v_{ez} + \boldsymbol{\Omega}_e (\partial_t + \nu_e) \boldsymbol{\nabla} \cdot \hat{\mathbf{z}} \times [\boldsymbol{\nabla} \cdot (n_e \mathbf{v}_e \mathbf{v}_e)] \\
&\qquad\quad + (\partial_t + \nu_e)^2 \boldsymbol{\nabla} \cdot [\boldsymbol{\nabla} \cdot (n_e \mathbf{v}_e \mathbf{v}_e)]\} \\
&\qquad -\frac{e}{m_e} \{[(\partial_t + \nu_e)^2 \boldsymbol{\nabla} + \boldsymbol{\Omega}_e^2 \boldsymbol{\nabla}_z] \cdot (n_s \mathbf{E}_p) - \boldsymbol{\Omega}_e (\partial_t + \nu_e) \hat{\mathbf{z}} \cdot (\boldsymbol{\nabla} n_s \times \mathbf{E}_p)\},
\end{aligned} \tag{6}$$

where $\omega_p = (4\pi n_0 e^2/m_e)^{1/2}$ is the electron plasma frequency.

The terms on the right-hand side of (6) are assembled into four groups of terms. The first two groups contain linear response terms and the last two contain coupling

https://doi.org/10.1017/S0022377801001477 Published online by Cambridge University Press

terms. The contribution to the parametric coupling from the third group of terms is much smaller than that from those in the fourth group, and hence the coupling terms in the third group will be neglected. Using (1), (3), and (6), the coupled mode equation for the Langmuir sideband is then derived to be (Kuo et al. 1983)

$$\{[(\partial_t+\nu_e)^2+\Omega_e^2](\partial_t^2+\nu_e\partial_t+\omega_p^2-3v_{te}^2\nabla^2)\nabla^2-\Omega_e^2(\omega_p^2-3v_{te}^2\nabla^2)\nabla_\perp^2\}\phi$$
$$=\omega_p^2\left\{[(\partial_t+\nu_e)^2\boldsymbol{\nabla}+\Omega_e^2\boldsymbol{\nabla}_z]\cdot\left\langle\frac{\mathbf{E}_p n_e^*}{n_0}\right\rangle\right.$$
$$\left.-\boldsymbol{\Omega}_e(\partial_t+\nu_e)\hat{\mathbf{z}}\cdot\left\langle\boldsymbol{\nabla}\left(\frac{n_e^*}{n_0}\right)\times\mathbf{E}_p\right\rangle\right\}, \tag{7}$$

where $\langle\ \rangle$ stands for a filter, which keeps only terms having the same phase function as that of the corresponding physical quantity on the left-hand side of (7). It is noted that one of the lowest-order kinetic effects (Dysthe et al. 1984), i.e., the electron Landau damping, is included in (7) through ν_e.

Both electrons and ions can effectively respond to low-frequency wave fields. Hence, the formulation of the coupled mode equation needs to include both electron and ion fluid equations. Since electrons and ions tend to move together, the formulation can be simplified by introducing the quasineutrality condition: $n_{si}\approx n_{se}=n_s$. The ion fluid equations are similar to (1) and (2), except that the subscript e is changed to i and the charge e changed to $-e$. Moreover, the collision frequencies are replaced by $\nu_{ei}=\nu_e-\nu_i$ and $\nu_{ie}=\nu_i-\nu_e$ in the electron and ion fluid equations, respectively. The coupled mode equation for the low-frequency mode is derived as (Kuo 1996)

$$\left\{\partial_t^3(\partial_t+\nu_e)[\partial_t(\partial_t+\nu_i)-C_s^2\nabla^2+\boldsymbol{\Omega}_e\boldsymbol{\Omega}_i]\nabla_\perp^2\right.$$
$$\left.+\Omega_e^2\{(\partial_t^2+\Omega_i^2)[\partial_t(\partial_t+\nu_i)-C_s^2\nabla^2]+\Omega_i^2C_s^2\nabla_\perp^2\}\right\}\nabla_z^2\left(\frac{n_e}{n_0}\right)$$
$$=\frac{m}{M}[(\partial_t^2+\Omega_i^2)\nabla_z^2+\partial_t^2\nabla_\perp^2]$$
$$\times\left[\partial_t(\partial_t+\nu_e)\boldsymbol{\nabla}_\perp\cdot\mathbf{a}_{p\perp}+\Omega_e^2\left(\partial_z a_{pz}-\frac{\partial_t\boldsymbol{\nabla}\cdot\mathbf{J}_B}{n_0}\right)\right.$$
$$\left.-\boldsymbol{\Omega}_e\partial_t\boldsymbol{\nabla}\cdot\mathbf{a}_p\times\hat{\mathbf{z}}\right], \tag{8}$$

where

$$\nu_i=\left(\frac{\pi}{2}\right)^{1/2}k_sC_s\left(\frac{T_e}{T_i}\right)^{3/2}\exp\left[-\frac{1}{2}\left(3+\frac{T_e}{T_i}\right)\right]$$

is the ion Landau-damping rate, $\boldsymbol{\Omega}_i$ is the ion cyclotron frequency, $C_s=[(T_e+3T_i)/M]^{1/2}$ is the ion acoustic speed, and M is the ion (O^+) mass; $\mathbf{a}_p=\langle\mathbf{v}_e\cdot\boldsymbol{\nabla}\mathbf{v}_e\rangle$ and $\mathbf{J}_B=\langle n_e\mathbf{v}_e\rangle$. Both (7) and (8) will be simplified for each parametric coupling process to be studied in the following sections.

3. Parametric decay instability (PDI)

As an HP heating wave of right-hand circular polarization propogates toward its reflection height, its wavevector and group velocity decrease gradually to zero. The accumulation of its energy flux leads to significant enhancement in the wave electric field. The wave polarization is also changed to the O-mode polarization in

https://doi.org/10.1017/S0022377801001477 Published online by Cambridge University Press

that region. Thus, the HF heating-wave electric field exceeds the threshold fields of many parametric instabilities. Among them, the PDI is a favorable one excited by the heating wave, as will be shown in the following and as also evidenced by experimental results. It is a process effectively converting the transmitted electromagnetic wave energy into plasma wave energy.

Consider the decay of a dipole pump $\mathbf{E}_p(\omega_0, \mathbf{k}_p = 0)$ into a Langmuir sideband $\phi(\omega, \mathbf{k})$ and an ion acoustic decay mode $n_s(\omega_s, \mathbf{k}_s)$, where $\mathbf{E}_p$ $(= \hat{\mathbf{z}}E_p)$, ϕ, and n_s denote the pump-wave field, the sideband's electrostatic potential, and the ion acoustic mode's density perturbation, respectively. The frequency and wavevector matching conditions are

$$\omega_0 = \omega + \omega_s^*, \qquad k_p = 0 = \mathbf{k} + \mathbf{k}_s,$$

where $\mathbf{k} = \hat{\mathbf{z}}k_z + \hat{\mathbf{x}}k_\perp$ and a background magnetic field $\mathbf{B}_0 = \hat{\mathbf{z}}B_0$ is assumed; the matching conditions lead to $\omega = \omega_0 - \omega_s^*$ and $\mathbf{k}_s = -\mathbf{k}$.

The coupled mode equation (7) for the Langmuir sideband is then reduced to

$$\{[(\partial_t + \nu_e)^2 + \Omega_e^2](\partial_t^2 + \nu_e\partial_t + \omega_p^2 - 3v_{te}^2\nabla^2)\nabla^2 - \Omega_e^2(\omega_p^2 - 3v_{te}^2\nabla^2)\nabla_\perp^2\}\phi$$
$$= \omega_p^2[(\partial_t + \nu_e)^2 + \Omega_e^2]\partial_z\left\langle \frac{E_p n_s^*}{n_0}\right\rangle. \tag{9}$$

As the oblique propagation angle θ (with respect to the magnetic field) of the Langmuir sideband is not close to 90°, the ion acoustic decay mode is mainly driven by the parallel (to the magnetic field) component of the ponderomotive force induced by high-frequency wave fields. Moreover, $|\partial_t^2\nabla_\perp^2| \ll |\Omega_e^2\nabla_z^2|$; thus, the coupled mode equation (8) for the ion acoustic mode is reduced to

$$\{(\partial_t^2 + \Omega_i^2)[\partial_t(\partial_t + \nu_i) - C_s^2\nabla^2] + \Omega_i^2C_s^2\nabla_\perp^2\}\nabla_z^2\left(\frac{n_s}{n_0}\right)$$
$$= \frac{m}{M}[(\partial_t^2 + \Omega_i^2)\nabla_z^2 + \partial_t^2\nabla_\perp^2]\partial_z\mathbf{a}_{pz} \tag{10}$$

where $a_{pz} = \partial_z\langle\frac{1}{2}v_{ez}^2\rangle$ for the present case where $\mathbf{E}_p = \hat{\mathbf{z}}E_p$.

Let $E_p = \mathscr{E}_p\exp(-i\omega_0 t) + \text{c.c.}$ and express the spatial and temporal variation of perturbations in the form $p = \mathscr{p}\exp[i(\boldsymbol{\kappa}\cdot\mathbf{r} - \tilde{\omega}t)]$, with $\mathscr{p} = \varphi$ and $\mathscr{n}$ for $p = \phi$ and n, respectively, and where $\boldsymbol{\kappa}$ and $\tilde{\omega}$ are the appropriate wavevector and frequency of each perturbation. Then (9) and (10) are reduced, respectively, to

$$[\omega(\omega + i\nu_e) - \omega_{k\theta}^2]\varphi = \frac{ik_z}{k^2}\omega_p^2\mathscr{E}_p\frac{\mathscr{n}_s^*}{n_0} \tag{11}$$

and

$$[\omega_s(\omega_s + i\nu_i) - k^2C_s^2]\frac{\mathscr{n}_s}{n_0} = \frac{ik_zk^2\omega_p^2}{4\pi n_0M\omega_0\omega}\mathscr{E}_p\varphi^* \tag{12}$$

where

$$\omega_{k\theta}^2 = \omega_p^2 + 3k^2v_{te}^2 + \Omega_e^2\sin^2\theta, \qquad \sin^2\theta = \frac{k_\perp^2}{k^2}.$$

Equations (11) and (12) are combined to obtain the dispersion relation for the PDI:

$$[\omega(\omega + i\nu_e) - \omega_{k\theta}^2][\omega_s^*(\omega_s^* - i\nu_i) - k^2C_s^2] = \frac{k_z^2\omega_p^4}{4\pi n_0M\omega_0\omega}|\mathscr{E}_p|^2. \tag{13}$$

We now set $\omega = \omega_r + i\gamma_k$ and $\omega_s = \omega_{sr} + i\gamma_k$ in (13) and evaluate the threshold field $\mathscr{E}_{p\text{th}}(k, \theta)$ and growth rate $\gamma_k(\theta)$ of the instability excited in the matching

https://doi.org/10.1017/S0022377801001477 Published online by Cambridge University Press

height h_1 of the (k_1, θ_1) Langmuir wave, i.e., in the height region where $\omega_r^2 = \omega_1^2 = \omega_p^2(h_1) + 3k_1^2 v_{te}^2 + \Omega_e^2 \sin^2\theta_1$, and the sideband and decay wave of the instability are the driven waves, rather than the eigenmodes of the plasma. The results are

$$|\mathscr{E}_{p\mathrm{th}}(k, \theta; k_1, \theta_1)| = \left(1 + \frac{\Delta\omega_1^4}{\omega_0^2 \nu_e^2}\right)^{1/2} \left(\frac{mM}{e^2}\right)^{1/2} \frac{(\nu_e \nu_i \omega_{sr} \omega_0^3)^{1/2}}{k \cos\theta \omega_p} \tag{14}$$

and

$$\gamma_k \approx \left[\frac{\nu_e \nu_i}{4}\left(\frac{\mathscr{E}_p}{\mathscr{E}_{p\mathrm{th}}}\right)^2 + \frac{(\nu_e - \nu_i)^2}{16}\right]^{1/2} - \frac{\nu_e + \nu_i}{4} \tag{15}$$

where

$$\Delta\omega_1^2 = \omega_1^2 - \omega_{k\theta}^2 = 3(k_1^2 - k^2) v_{te}^2 + \Omega_e^2(\sin^2\theta_1 - \sin^2\theta),$$

$$\omega_{sr}^2 = k^2 C_s^2 + \frac{\omega_{sr} \nu_i \Delta\omega_1^2}{\omega_1 \nu_e}.$$

It is shown by (14) that the threshold field varies with the propagation angle θ and wavelength λ_1 of the Langmuir sideband as well as the location of excitation. When the instability is excited at the matching height h of its Langmuir sideband (k, θ), i.e., $\Delta\omega_1 = 0$, the threshold field is the minimum given by

$$|\mathscr{E}_{p\mathrm{th}}(k, \theta)|_m = \left(\frac{mM}{e^2}\right)^{1/2} \frac{(\nu_e \nu_i \omega_{sr} \omega_0^3)^{1/2}}{k \cos\theta\, \omega_p}. \tag{16}$$

In the Arecibo heating experiments, the parameters are $\omega_0/2\pi = 5.1\,\mathrm{MHz}$, $\Omega_e/2\pi = 1.06\,\mathrm{MHz}$, $\nu_e = 500\,\mathrm{Hz}$, $v_{te} \approx 1.3 \times 10^5\,\mathrm{m\,s^{-1}}$, $C_s \approx 1.4 \times 10^3\,\mathrm{m\,s^{-1}}$, and $k_0 \approx 4\pi$ (i.e., $\lambda_\parallel = 0.495\,\mathrm{m} = \lambda_R/(2\sin\theta_m)$, where $\lambda_R = 0.7\,\mathrm{m}$ is the wavelength of the 430 MHz radar signal and $\theta_m = 50°$ is the magnetic dip angle). The minimum threshold field $|\mathscr{E}_{p\mathrm{th}}(k_0, 0)|_m$ for the $(k_0, 0)$ line evaluated from (16) is about $0.07\,\mathrm{V\,m^{-1}}$.

In the Tromsø heating experiments, the parameters are $\omega_0/2\pi = 4\,\mathrm{MHz}$, $\Omega_e/2\pi = 1.35\,\mathrm{MHz}$, $\nu_e = 1\,\mathrm{kHz}$, $v_{te} \approx 1.8 \times 10^5\,\mathrm{m\,s^{-1}}$, $C_e \approx 1.66 \times 10^3\,\mathrm{m\,s^{-1}}$, and $k_{01} = 12.17\pi$ (i.e., $\lambda_{\parallel 1} = 0.1644\,\mathrm{m}$, corresponding to 933 MHz radar) or $k_{02} = 2.92\pi$ (i.e., $\lambda_{\parallel 2} = 0.685\,\mathrm{m}$ corresponding to 224 MHz radar). The minimum threshold fields $|\mathscr{E}_{p\mathrm{th}}(k_{01}, 0)|_m$ for the $(k_{01}, 0)$ line and $|\mathscr{E}_{p\mathrm{th}}(k_{02}, 0)|_m$ for the $(k_{02}, 0)$ line evaluated from (16) are about $0.16\,\mathrm{V\,m^{-1}}$ and $0.14\,\mathrm{V\,m^{-1}}$, respectively.

The minimum threshold field $|\mathscr{E}_{p\mathrm{th}}(k_1, \theta_1)|_m = |\mathscr{E}_{p\mathrm{th}}(\theta_1| \propto 1/\cos\theta_1$, depends weakly on the oblique propagation angle θ_1 of the Langmuir sideband. The growth rate in the strong-pump-field case, i.e., $(\mathscr{E}_p/\mathscr{E}_{p\mathrm{th}})^2 \gg 1$, is proportional to $k_1^{1/2}\cos\theta_1$. In the same region, the nonresonant (k, θ) sideband can also be excited. The threshold field of the instability is increased by a mismatch factor $(1 + \Delta\omega_1^4/\omega_0^2\nu_e^2)^{1/2}\, k_1^{1/2} \cos\theta_1/k^{1/2}\cos\theta$, and consequently the growth rate of the instability decreases as the mismatch frequency $|\Delta\omega_1|$ of the sideband increases. Nonetheless, the excited Langmuir waves are expected to have a spectral and angular distribution as well as a spatial distribution over an altitude region.

However, only those spectral lines termed HFPLs, having a wavenumber twice that of the probing radar signal and pointing in a direction parallel or antiparallel to the pointing direction of the radar, can effectively backscatter the radar signal. Thus, the HFPLs excited by the PDI process do not have the lowest threshold field and highest growth rate. They are most favorably excited in a region called the

'matching height', which is below the reflection height of the O-mode heating wave by a distance $d \approx L(12k_R^2 v_{te}^2 + \Omega_e^2 \sin^2\theta_0)/\omega_0^2$, where L is the linear scale length of the background plasma, k_R is the wavenumber of the backscatter radar signal, and θ_0 is the conjugate angle to the magnetic dip angle θ_m. As the Langmuir waves excited by the PDI grow to large amplitudes, they become pumps of secondary parametric instabilities, which broaden the spectral and angular distribution as well as the frequency bandwidth of Langmuir waves.

4. Spatial distribution of the oscillating two-stream instability (OTSI)

HF heating waves can also excite the OTSI. In the following, we show that, due to the geomagnetic field, the OTSI can be excited in a sizable region below the HF reflection height. This is in contrast to the unmagnetized case, where the OTSI can only be excited in a narrow region near the HF reflection height. The wavenumber spectrum of Langmuir sidebands excited in each height region, again, has an angular distribution centered at an oblique propagation angle (with respect to the magnetic field) of a Langmuir eigenmode at that height.

The OTSI process involves the decay of a dipole pump $\mathbf{E}_p(\omega_0, \mathbf{k}_p = 0)$ into two Langmuir sidebands $\phi_1(\omega_1, \mathbf{k}_1)$ and $\phi_1'(\omega_1', \mathbf{k}_1')$ and a purely growing mode n_s ($\omega_s = i\gamma_s$, $\mathbf{k}_s$), where $\mathbf{E}_p = \hat{\mathbf{z}}E_p$, ϕ_1 and ϕ_1', and n_s are the pump-wave field, the sidebands' electrostatic potentials, and the purely growing mode's density perturbation, respectively, and γ_s is the growth rate of the instability. The frequency and wavevector matching conditions imposed by this parametric coupling process are given by

$$\omega_0 = \omega_1 + \omega_s^* = \omega_1' - \omega_s, \qquad \mathbf{k}_p = 0 = \mathbf{k}_1 + \mathbf{k}_s = \mathbf{k}_1' - \mathbf{k}_s,$$

where $\mathbf{k}_1 = \hat{\mathbf{z}}k_0 + \hat{\mathbf{x}}k_\perp$ and, again, a background magnetic field $\mathbf{B}_0 = \hat{\mathbf{z}}B_0$ is assumed. The matching conditions lead to $\omega_1 = \omega_1' = \omega_0 + i\gamma_s$ and $\mathbf{k}_1' = \mathbf{k}_s = -\mathbf{k}_1$. From (7), the coupled mode equations for Langmuir sidebands are

$$\{[(\partial_t + \nu_e)^2 + \Omega_e^2](\partial_t^2 + \nu_e\partial_t + \omega_p^2 - 3v_{te}^2\nabla^2)\nabla^2 - \Omega_e^2(\omega_p^2 - 3v_{te}^2\nabla^2)\nabla_\perp^2\}\phi_{1\pm} = \omega_p^2[(\partial_t + \nu_e)^2 + \Omega_s^2]\partial_z \left\langle \frac{E_p n_{s\pm}}{n_0} \right\rangle, \tag{17}$$

where the notation $\phi_{1+} = \phi_1$, $\phi_{1-} = \phi_1'$, and $n_{s+}^* = n_s = n_{s-}$ is used.

The parallel (to the magnetic field) component of the wavevector of the short-scale purely growing mode is not negligibly small; thus, the short-scale purely growing mode, similar to the ion acoustic mode, is also mainly driven by the parallel component of the ponderomotive force induced by the high-frequency wave fields. Therefore, the coupled mode equation for the purely growing mode has the same form as (10).

Equations (17) and (10) are analyzed in the same way as (9) and (10). The dispersion relation of the OTSI is then derived to be

$$\{(\gamma_s^2 + \Omega_i^2)[\gamma_s(\gamma_s + \nu_i) + k_1^2 C_s^2] - \Omega_i^2 k_\perp^2 C_s^2\} = \frac{2e^2}{mM} k_1^2 \cos^2\theta(\gamma_s^2 + \Omega_i^2\cos^2\theta)\frac{\Delta\omega^2}{\Delta\omega^4 + \omega_0^2(2\gamma_s + \nu_e)^2}|\mathscr{E}_p|^2, \tag{18}$$

where

$$\Delta\omega^2 = \omega_p^2 + 3k_1^2 v_{te}^2 + \Omega_s^2\sin^2\theta - \omega_0^2, \qquad \theta = \sin^{-1}\left(\frac{k_\perp}{k_1}\right).$$

https://doi.org/10.1017/S0022377801001477 Published online by Cambridge University Press

We first set $\gamma_s = 0$ in (18) to determine the threshold condition of the instability. The threshold field is obtained to be

$$|\mathscr{E}_p(\theta)|_{\rm th} = \left(\frac{mM}{2e^2}\right)^{1/2} C_s \left(\frac{\Delta\omega^4 + \omega_0^2\nu_e^2}{\Delta\omega^2}\right) \frac{1}{\cos\theta}. \tag{19}$$

Similar to (14) for the PDI, (19) shows that the threshold field of the OTSI also varies with the propagation angle θ and wavelength λ_1 of the Langmuir sidebands as well as the location of excitation. For each propagation angle θ and wavelength λ_1, the instability has the minimum threshold field

$$|\mathscr{E}_p(k_1,\theta)|_m = \left(\frac{mM}{e^2}\right)^{1/2} \frac{C_s(\omega_0\nu_e)^{1/2}}{\cos\theta}, \tag{20}$$

when it is excited in a preferential height layer with $\Delta\omega^2(k_1,\theta) = \omega_0\nu_e$, i.e., $\omega_p^2(h) = \omega_p^2(k_1,\theta) = \omega_0(\omega_0+\nu_e) - 3k_1^2v_{te}^2 - \Omega_e^2\sin^2\theta$, where h is the altitude of the preferential layer. In other words, the spectral lines of the Langmuir sidebands excited by the OTSI have an angular ((θ) and a spectral (k_1) distribution, as well as a spatial (h) distribution in a finite altitude region. This minimum threshold field (20) increases with the oblique propagation angle θ of (k_1,θ) lines, but it is independent of k_1. The altitude h of the preferentially excited region for (k_1,θ) lines moves downward as the oblique propagation angle θ of these lines increases.

Considering a family of spectral lines having $\mathbf{k}_0 = \hat{\mathbf{z}}k_0$ as the common parallel component of their wave vectors, the oblique angle θ of (k_1,θ) lines increases with $k_\perp$ (i.e., $\mathbf{k}_1 = \mathbf{k}_0 + \mathbf{k}_\perp$). The threshold fields for (k_1,θ) lines excited in the layer $h = h_0$ with $\omega_p(h_0) = \omega_p(k_0,0)$ and in the layer $h = h_1$ with $\omega_p(h_1) = \omega_p(k_1,\theta)$ (i.e., near the matching height), expressed in terms of the minimum threshold field $|\mathscr{E}_p(k_0,0)|_m$ of the $(k_0,0)$ line, are

$$|\mathscr{E}_p(k_1,\theta)|_{\rm th} = f(\theta,0)|\mathscr{E}_p(k_0,0)|_m$$

and

$$|\mathscr{E}_p(k_1,\theta)|_m = \frac{|\mathscr{E}_p(k_0,0)|_m}{\cos\theta},$$

respectively, where

$$|\mathscr{E}_p(k_0,0)|_m = \left(\frac{mM}{e^2}\right)^{1/2} C_s(\omega_0\nu_e)^{1/2},$$

$$f(\theta,0) = \frac{1}{\cos\theta}\left[1 + \frac{\Delta\omega_m^4}{2\omega_0\nu_e(\omega_0\nu_e + \Delta\omega_m^2)}\right]^{1/2}, \tag{21}$$

and

$$\Delta\omega_m^2 = \Omega_e^2\sin^2\theta + 3k_0^2V_{te}^2\tan^2\theta.$$

Using the parameters of the Arecibo and Tromsø heating experiments given in Sec. 2, the minimum threshold fields for the $(k_0,0)$ lines, at the two respective heating sites, evaluated from (20) are about $0.17\,\mathrm{V\,m^{-1}}$ and $0.255\,\mathrm{V\,m^{-1}}$, respectively, which are about 2.4 and 1.65 times larger than those of the PDI at the two sites exciting similar $(k_0,0)$ plasma lines in the corresponding nearby regions.

The strong increasing dependence of $f(\theta,0)$ on θ, from (21), however, indicates that the threshold field of (k_1,θ) lines excited in the same height layer $h = h_0$ with $\omega_p(h_0) = \omega_p(k_0,0)$ increases rapidly with the obliquely propagating angle θ

https://doi.org/10.1017/S0022377801001477 Published online by Cambridge University Press

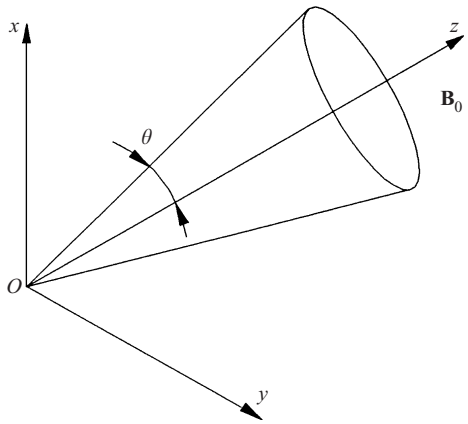

Figure 1. Angular distribution of Langmuir sidebands excited by the OTSI in the region near the reflection height of the O-mode HF heating wave.

of (k_1, θ) lines. Thus, the angular distribution of the spectral lines of the Langmuir sidebands excited by the OTSI in the region near the HF wave reflection height, i.e., $h = h_0$, is expected to be confined in narrow cones around the geomagnetic field, as shown in Fig. 1. On the other hand, $f(\theta, 0)\cos\theta$ also increases rapidly from 1 with the obliquely propagating angle θ, for example, in the Arecibo case $f(\theta, 0)\cos\theta = 27.3$ for $\theta = 40°$ and in the Tromsø case, $f(\theta, 0)\cos\theta = 13.75$ and 8.4 for $\theta = 12°$ and $k_0 = k_{01}$ (corresponding to 933 MHz radar) and k_{02} (corresponding to 224 MHz radar), respectively. Thus, in Arecibo, the threshold field for $(k_1, 40°)$ lines excited at their matching layer $h = h_1$ with $\omega_p(h_1) = \omega_p(k_1, 40°)$ is $0.22\,\mathrm{V\,m^{-1}}$, which is 27.3 times lower than the threshold field $6.06\,\mathrm{V\,m^{-1}}$ for the same lines excited in the layer $h = h_0$. In Tromsø, the threshold field for $(k_1, 12°)$ lines excited at their matching layer $h = h_1$ with $\omega_p(h_1) = \omega_p(k_1, 12°)$, for both $k_1 = k_{11}$ and k_{12}, is $0.26\,\mathrm{V\,m^{-1}}$, which is 13.75 and 8.4 times lower than the threshold fields $3.575\,\mathrm{V\,m^{-1}}$ and $2.184\,\mathrm{V\,m^{-1}}$ for the same lines excited in the layers $h = h_{01}$ and h_{02}, respectively.

The results clearly show that the oblique-angle line is preferentially excited in its matching height region, rather than in the region near the HF reflection height. However, in the Tromsø heating experiments, the OTSI was suppressed by instabilities draining heating wave energy in the upper-hybrid resonance region. As the excitation region moves downward to the matching height h_{10} of the (k_{10}, θ_0) lines, the threshold field of (k_1, θ) lines becomes

$$|\mathscr{E}_p(k_1, \theta)|_{\mathrm{th}} = f_1(\theta, \theta_0)|\mathscr{E}_p(k_0, 0)|_m,$$

where

$$f_1(\theta, \theta_0) = \frac{1}{\cos\theta}\left[1 + \frac{(\Delta\omega_m^2 - \Delta\omega_{m0}^2)^2}{2\omega_0\nu_e(\omega_0\nu_e + \Delta\omega_m^2 - \Delta\omega_{m0}^2}\right]^{1/2} \tag{22}$$

and

$$\Delta\omega_{m0}^2 = \Omega_e^2 \sin^2\theta_0 + 3k_0^2 v_{te}^2 \tan^2\theta_0.$$

Thus, the angular distribution of Langmuir sidebands excited in this layer becomes a hollow shape from θ_1 to θ_2, where $\theta_1 \approx \theta_0$ (i.e., lines around $\theta = 0$ cannot be excited), and has a narrower angular range, as shown in Fig. 2. For example, in

https://doi.org/10.1017/S0022377801001477 Published online by Cambridge University Press

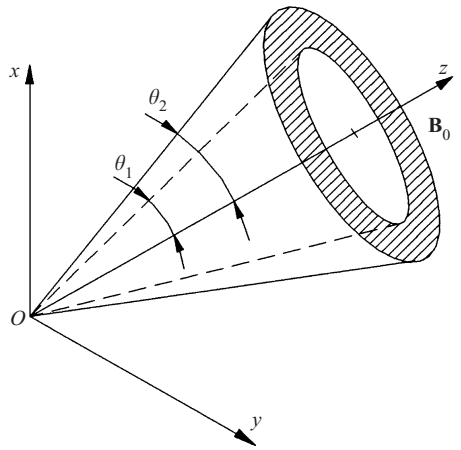

Figure 2. Angular distribution of Langmuir sidebands excited by the OTSI in the matching height region of the obliquely propagating Langmuir sidebands at the angle θ_0.

the Arecibo case, the threshold field evaluated from (19) for $\theta = 10°$ lines excited in the region near the HF reflection height (i.e., $h = h_0$) is about $1.22\,\mathrm{V\,m^{-1}}$, which can be exceeded by the HF wave field after the swelling factor is included. Using the parameters of the Tromsø heating experiments, this threshold field for lines having $\theta = 10°$ and $k_0 = k_{02}$ (corresponding to 224 MHz radar) is about the same, but it increases considerably for lines having $\theta = 10°$ and $k_0 = k_{01}$ (corresponding to 933 MHz radar). The angular distribution of excited Langmuir sidebands at the Tromsø site is expected to be much narrower than that at the Arecibo site.

The analysis presented in this section shows that the OTSI can occur in a much wider altitude range than was previously thought. Its effect on geophysical processes during HF heating experiments should not only be evaluated locally in the region near the HF wave reflection layer.

5. Cascade of PDI and OTSI-excited Langmuir waves via ion acoustic waves

In the preceding two sections, we have shown that Langmuir waves excited by the OTSI and PDI in the region below the HF wave reflection height have an angular distribution around the geomagnetic field. These waves have a frequency either equal to the frequency of the HP wave or lower than that of the HP wave by an ion acoustic wave frequency. As these Langmuir waves grow to large amplitudes, they become pump waves to excite secondary parametric instabilities. The secondary parametric decay instability considered in this section is the decay of a Langmuir pump, excited by the OTSI or by the PDI, into an ion acoustic decay mode and a Langmuir sideband. Through this process, as shown in the following, those Langmuir waves excited by the OTSI and PDI can cascade several times to broaden the frequency spectrum.

The secondary parametric decay instability can occur at the same location as that of the primary parametric decay instability, which generates the mother line of the first cascade line in the HFPLs. However, the cascading process is a nonresonant decay, namely, the sideband of the secondary parametric decay instability cannot satisfy the local dispersion relation of the Langmuir wave. This is because

the HFPLs have the same wavevector but different frequencies. In order to achieve a resonant decay, the mother line as the pump has to propagate downward to a location where the sideband of the secondary parametric decay instability is also a local plasma mode. Thus, different cascade steps occur at different altitudes, and the wavelength of the mother line in each cascade step is slightly shorter than that of the daughter line. In this case, the propagation loss of each mother line propagating from its generation region to the resonance region of its daughter line has to be taken into account in determining the threshold field of each resonant cascade step.

This secondary parametric decay instability excited by the OTSI- or PDI-excited Langmuir waves is analyzed first. It represents the first cascade process. The decay mode is the ion acoustic wave, which propagates in the same direction as that of the pump wave and has a wavelength about half that of the pump wave. The Langmuir sideband propagates in the direction opposite to that of the pump wave and has a wavelength about the same as that of the pump wave. This Langmuir sideband is called the first cascade line of a Langmuir wave excited by the OTSI or PDI. It will continue to cascade through the same instability process if its saturation amplitude exceeds the instability threshold. The analysis for the first cascade process can easily be generalized for the subsequent cascade. The number of cascades of Langmuir waves excited by the OTSI and PDI is the focus of the following analysis.

Considering the parametric decay of a Langmuir pump wave $\phi(\omega, \mathbf{k})$ into a Langmuir sideband $\phi_1(\omega_1, \mathbf{k}_1)$ and an ion acoustic mode $n_{s1}(\omega_{s1}, \mathbf{k}_{s1})$, the frequency and wavevector matching conditions are

$$\omega = \omega_1 + \omega_{s1}^*, \qquad \mathbf{k} = \mathbf{k}_1 + \mathbf{k}_{s1},$$

where $\mathbf{k}_1 \approx -\mathbf{k}$ and thus $\mathbf{k}_{s1} \approx 2\mathbf{k}$.

Because the Langmuir pump is an electrostatic mode, both parallel and perpendicular divergent components of the first term on the right-hand side of (7) contribute to the coupling. Moreover, the coupling function on the right-hand side of (10), $a_{pz} = \langle \mathbf{v}_e \cdot \boldsymbol{\nabla} v_{ez} \rangle = \partial_z \langle \frac{1}{2} v_{ez}^2 \rangle + \langle \mathbf{v}_{e\perp} \cdot \boldsymbol{\nabla}_\perp v_{ez} \rangle$, also contains an extra term. Including these additional coupling terms, the coupled mode equations for the Langmuir sideband and ion acoustic decay mode become

$$[\omega_1(\omega_1 + i\nu_e) - \omega_{k\theta}^2]\varphi_1 = \omega_p^2 g(\theta, \omega)\varphi \frac{n_{s1}^*}{n_0} \tag{23}$$

and

$$[\omega_{s1}(\omega_{s1} + i\nu_i) - 4k^2 C_s^2]\frac{n_{s1}}{n_0} = \frac{k^4 g(\theta, \omega)\omega_p^2}{\pi n_0 M \omega^2}\varphi\varphi_1^*, \tag{24}$$

where $k_1 \approx k$, $k_{s1} \approx 2k$, and $|\omega_1| \approx \omega$ are assumed;

$$g(\theta, \omega) = \cos^2\theta + \frac{\sin^2\theta\,\omega^2}{\omega^2 - \Omega_e^2}$$

and $\omega \approx \omega_{k\theta}$.

From (23) and (24), the dispersion relation of the instability is derived to be

$$[\omega_1(\omega_1 + i\nu_e) - \omega_{k\theta}^2][\omega_{s1}^*(\omega_{s1}^* - i\nu_i) - 4k^2 C_s^2] = k^4 g(\theta, \omega)^2 \frac{\omega_p^4}{\pi n_0 M \omega^2}|\varphi^2|. \tag{25}$$

Equation (25) is analyzed for the cases of resonant and nonresonant decay.

https://doi.org/10.1017/S0022377801001477 Published online by Cambridge University Press

5.1. Resonant decay

Introducing $\omega_{s1} = 2kC_s + i\gamma_1$ and $\omega_1 = \omega_{k\theta} + i\gamma_1$ in (25), where γ_1 is the linear growth rate of the instability, it becomes

$$2kC_s\omega_{k\theta}(2\gamma_1 + \nu_e)(2\gamma_1 + \nu_i) = k^4 g(\theta, \omega_{k\theta})^2 \frac{\omega_p^4}{\pi n_0 M \omega_{k\theta}^2} |\varphi|^2. \tag{26}$$

Setting $\gamma_1 = 0$ in (26), the threshold field of the instability is obtained as

$$k|\varphi|_{\text{th}} = k|\varphi|_0 \approx \frac{|\mathscr{E}_{p\text{th}}(\theta)| \cos\theta}{\sqrt{2} g(\theta, \omega_{k\theta})}, \tag{27}$$

where

$$|\varphi|_0 = \frac{(2\pi n_0 M k C_s \omega_{k\theta}^3 \nu_e \nu_i)^{1/2}}{k^2 g(\theta, \omega_{k\theta}) \omega_p^2}.$$

The threshold field (27) for the first cascade step of the Langmuir sidebands of the OTSI or PDI through a resonant decay process is quite small. A similar analysis leads to about the same threshold field for the subsequent cascades. However, the Langmuir pump wave has to propagate downward a distance from its excitation altitude z_0 to the decay altitude z_1. When the wave propagates outside of its excitation region, its field amplitude decays exponentially due to the collision and collisionless losses. Therefore, the actual threshold field is increased by an exponential factor $e^{\alpha\Delta z}$, where α is the spatial damping rate of the Langmuir wave and $\Delta z = |z_0 - z_1|$ is the distance between the two altitudes.

The spatial damping rate can be derived from the dispersion relation $\omega(\omega + i\nu_e) - \omega_{k\theta}^2 = 0$, obtained from the left-hand side of (11), where ν_e is the total effective collision frequency including the Landau-damping effect. Setting $k = k_r + i\alpha$ in the dispersion relation for a real ω, the damping rate $\alpha \approx \nu_e/2v_g$ is derived, where $v_g = 3k_r v_{te}^2/\omega$ is the group velocity of the Langmuir wave. The distance Δz can be determined in terms of the inhomogeneous scale length L of the plasma density. Since the mother line and the daughter line in the HFPLs have the same wavevector at their respective originating altitudes z_0 and z_1, $\omega^2 - \omega_1^2 = \omega_p^2(z_0) - \omega_p^2(z_1)$, which leads to $\Delta z = 4\omega k_r C_s L/\omega_p^2(z_0)$. Hence, $\alpha\Delta z = 2C_s\nu_e\omega^2 L/3\omega_p^2 v_{te}^2 \geqslant 1$ for $L = 20$–50 km, $T_i \approx T_e$, and $\nu_e \geqslant 500$ Hz.

Normally, the daughter line saturates at about the same intensity level as that of the mother line in the excitation region of the daughter line. Thus, the spectral intensity ratio of the mother line to the daughter line in HFPLs will be about $e^{2\alpha\Delta z}$, which leads to about a 10 dB power difference. The same analysis and results are applicable for the subsequent cascades. Therefore, the spectral intensities of the cascade lines in HFPLs should decrease consecutively by a factor $e^{-2\alpha\Delta z}$ (i.e. 10 dB down consecutively) if they are generated by the resonant cascading process.

5.2. Nonresonant decay

Setting $\omega_{s1} = \omega_{s1r} + i\gamma_1$ and $\omega_1 = \omega_{k\theta} - \omega_{s1r} + i\gamma_1$ in (25) leads to two real equations:

$$(2\gamma_1 + \nu_e)[4k^2C_s^2 + \gamma_1(\gamma_1 + \nu_i) - \omega_{s1r}^2] = 2\omega_{s1r}^2(2\gamma_1 + \nu_i) \tag{28}$$

and

$$2\omega_{k\theta}\omega_{s1r}[4k^2C_s^2 + \gamma_1(\gamma_1 + \nu_i) - \omega_{s1r}^2] + \omega_{k\theta}\omega_{s1r}(2\gamma_1 + \nu_e)(2\gamma_1 + \nu_i)$$
$$= k^4 g(\theta, \omega_{k\theta})^2 \frac{\omega_p^4}{\pi n_0 M \omega_{k\theta}^2 |\varphi|^2} \tag{29}$$

https://doi.org/10.1017/S0022377801001477 Published online by Cambridge University Press

At the threshold field, $\gamma_1 = 0$. Thus, $\omega_{s1r}^2 = [\nu_e/(\nu_e + 2\nu_i)]4k^2C_s^2$ is obtained from (28), and the threshold field of the instability is obtained from (29) as

$$|\varphi|_{\rm th}^2 = \left[1 + \frac{16k^2C_s^2}{\nu_e(\nu_e + 2\nu_i)}\right]\left(\frac{\nu_e}{\nu_e + 2\nu_i}\right)^{1/2}|\varphi|_0^2$$
$$\approx \frac{8C_s^2\cos^2\theta}{[\nu_e(\nu_e + 2\nu_i)^3]^{1/2}}\,|\mathscr{E}_{p\rm th}(\theta)|^2, \tag{30}$$

where $\Omega_e^2 \ll \omega_{k\theta}^2$ has been used to simplify the result.

Equation (30) determines only the threshold field for exciting the first cascade line of the Langmuir sideband of the OTSI or PDI through a nonresonant decay process. However, the analysis can easily be extended to determine the threshold field for the excitation of the Nth cascade line $\phi_N(\omega_N, -\mathbf{k})$. In this case, the pump is the $(N-1)$th cascade line $\phi_{N-1}(\omega_{N-1}, \mathbf{k})$ and the decay mode is again an ion acoustic mode $n_{sN}(\omega_s, 2\mathbf{k})$. Equations (23) and (24) are generalized to become the coupled mode equations for the Nth cascade:

$$[\omega_N(\omega_N + i\nu_e) - \omega_{k\theta}^2]\varphi_N = \omega_p^2\varphi_{N-1}\frac{\mathscr{n}_{sN}^*}{n_0} \tag{31}$$

and

$$[\omega_{sN}(\omega_{sN} + i\nu_i) - 4k^2C_s^2]\frac{\mathscr{n}_{sN}}{n_0} = k^4g(\theta, \omega_{N-1})^2\frac{\omega_p^2}{\pi n_0 M\omega_{n-1}^2}\varphi_{N-1}\varphi_N^*. \tag{32}$$

Setting $\omega_{sN} \approx \omega_{sNr} + i\gamma_N$ and $\omega_N \approx \omega_{k\theta} - \sum_{q-1}^N \omega_{sqr} + i\gamma_N$ in (31) and (32), the dispersion relation for this cascade step is derived as

$$\left[i\omega_0(2\gamma_N + \nu_e) - 2\omega_0\sum_{q=1}^N \omega_{sqr}\right]$$
$$\times[-i\omega_{sNr}(2\gamma_N + \nu_i) + \omega_{sNr}^2 - 4k^2C_s^2 - \gamma_N(\gamma_N + \nu_i)]$$
$$= k^4g(\theta, \omega_0)^2\frac{\omega_p^4}{\pi n_0 M\omega_0^2}|\varphi_{N-1}|^2, \tag{33}$$

where $\omega_{k\theta} \approx \omega_0 \approx \omega_{N-1}$ are assumed.

Equation (33) is solved to determine the threshold field $|\varphi_{N-1}|_{\rm th}$ by setting $\gamma_N = 0$. The result is found to be

$$|\varphi_{N-1}|_{\rm th}^2 = \left[1 + \frac{16N^2k^2C_s^2}{\nu_e(\nu_e + 2N\nu_i)}\right]\left(\frac{\nu_e}{\nu_e + 2N\nu_i}\right)^{1/2}|\varphi|_0^2$$
$$\approx N^2\left(\frac{\nu_e + 2\nu_i}{\nu_e + 2N\nu_i}\right)^{3/2}|\varphi|_{\rm th}^2, \tag{34}$$

where $\sum_{q=1}^N \omega_{sqr} \approx N\omega_{sNr}$ and $16N^2k^2C_s^2/\nu_e(\nu_e + 2N\nu_i) \gg 1$ are assumed.

Consider two extreme cases that $\nu_e \gg 2N\nu_i$ and $\nu_e \ll 2N\nu_i$ for comparison; then (34) reduces to

$$|\varphi_{N-1}|_{\rm th}^2 \approx \begin{cases} N^2|\varphi|_{\rm th}^2 & \text{for } \nu_e \gg 2N\nu_i, \\ N^{1/2}|\varphi|_{\rm th}^2 & \text{for } \nu_e \ll 2N\nu_i. \end{cases} \tag{35}$$

The results presented in (35) suggest that the spectral features of the cascade plasma lines, produced via the ion acoustic decay process, depend strongly on ν_e/ν_i, i.e.,

https://doi.org/10.1017/S0022377801001477 Published online by Cambridge University Press

the latitude of the heating site, the time of the experiment, and the frequency of the heating wave. In general, Langmuir waves excited by the OTSI and PDI will cascade several times through the considered proces to broaden their frequency spectrum. However, the bandwidth of produced HFPLs is quite narrow, because the ion acoustic frequency is low and the achievable number of cascades is limited by the increasing dependence of the instability threshold on the number of cascades.

6. Cascade of Langmuir waves via the lower-hybrid decay mode

Langmuir waves excited in heating experiments by the OTSI in the region $h = h_0$ (where $\omega_p^2 = \omega_0(\omega_0 + \nu_e) - 3k_0^2 v_{te}^2$) near the HF reflection height have a small ($\approx 10°$–$20°$ for $|\mathscr{E}_p| \approx 2\,\mathrm{V\,m^{-1}}$) angular distribution around the geomagnetic field. These waves have the same frequency as the HF wave. Likewise, a similar spectral distribution of Langmuir waves can also be excited by the PDI – however, in the slightly lower region $h = h_p < h_0$, where $\omega_p^2 = \omega(\omega + \nu_e) - 3k_0^2 v_{te}^2$ and $\omega = \omega_0 - \omega_s$ is the frequency of the Langmuir wave. It takes a continuous cascade of Langmuir waves by secondary parametric instabilities to broaden the downshifted frequency spectrum of Langmuir waves. However, the permissible number of cascades and the required pump threshold field for producing a broadband of frequency-downshifted Langmuir waves depend on the secondary parametric instability process. For example, the secondary parametric decay instability considered in the preceding section, which decays a Langmuir pump wave into an ion acoustic decay mode and a Langmuir sideband, cannot significantly broaden the frequency spectrum of Langmuir waves. Thus, other processes were explored to account for the broad frequency-downshifted spectrum of HFPLs observed occasionally in recent Arecibo heating experiments. One feasible process, which could cascade Langmuir waves continuously in the same region (i.e., a nonresonant cascading process) to produce a broadband of frequency-downshifted Langmuir waves was found to be the decay of a Langmuir pump wave into a Langmuir sideband and a lower-hybrid decay mode. This decay process requires that the wavevectors of three waves be matched in three-dimensional space, rather than the conventional two-dimensional arrangement matching them on the plane of the pump wavevector and the geomagnetic field. Through the filamentation instability (Kuo et al. 1993) or scattering with the short-scale field-aligned density irregularities, some of these Langmuir waves were converted into plasma lines propagating at 40°, becoming detectable by the Arecibo 430 MHz backscatter radar. This process together with the OTSI were considered by Kuo and Lee (1999) to show the possible generation of a broad downshifted spectrum of HFPLs originating from the same altitude near the reflection height of the O-mode HF heating wave in the Arecibo heating experiments. However, it has been shown in the preceding sections that the 40° Langmuir sidebands contributing to HFPLs can also be directly generated by the OTSI as well as the PDI in the matching height regions of the respective sidebands. In the following, we show that the cascade of these 40° Langmuir sidebands, excited by either instability through the same secondary parametric instability considered by Kuo and Lee (1999), can also lead to a broad downshifted spectrum of HFPLs originating from the same altitude in the Arecibo heating experiments. However, this altitude is the matching height of the 40° Langmuir waves rather than that near the O-mode HF reflection height.

Considering the decay of a Langmuir pump $\phi_1(\omega_1, \mathbf{k}_1)$ into a Langmuir sideband $\phi_2(\omega_2, \mathbf{k}_2)$ and a lower-hybrid decay mode $n_3(\omega_3, \mathbf{k}_3)$ in a layer at $h = h_{10}$, where

https://doi.org/10.1017/S0022377801001477 Published online by Cambridge University Press

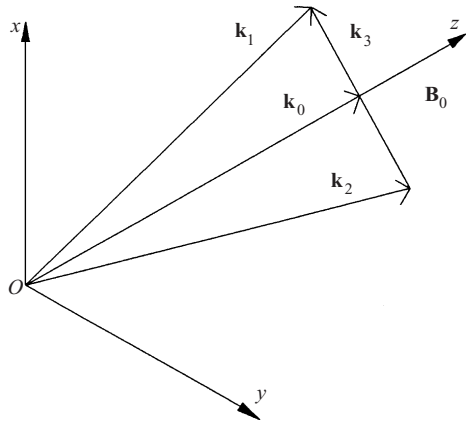

Figure 3. Wave vector matching diagram of the cascading via the proposed secondary parametric decay process.

$\omega_p^2(h_{10}) = \omega_0(\omega_0 + \nu_e) - 3k_{10}^2 v_{te}^2 - \Omega_e^2 \sin^2\theta_0$, the frequency and wavevector matching conditions are

$$\omega_1 = \omega_2 + \omega_3^*, \qquad \mathbf{k}_1 = \mathbf{k}_2 + \mathbf{k}_3,$$

where $\mathbf{k}_1 = \hat{\mathbf{z}}k_0 + \hat{\mathbf{x}}k_\perp$, $\mathbf{k}_2 = \hat{\mathbf{z}}(k_0 - k_z) + \hat{\mathbf{y}}k_\perp$, and thus $\mathbf{k}_3 = (\hat{\mathbf{x}} - \hat{\mathbf{y}})k_\perp + \hat{\mathbf{z}}k_z$; $k_\perp/k_0 = \tan\theta$ and $|k_z/k_\perp| \ll 1$. The wavevector matching condition is plotted in Fig. 3. It is noted that there will be no instability if $\mathbf{k}_1, \mathbf{k}_2$, and the z axis are in the same plane. This is because the product of the coupling terms of the two-coupled mode equations has a wrong sign. In other words, the proposed decay and cascading processes have to develop in three-dimensional space.

The cascading process is described as follows. When the $\mathbf{k}_2$ line grows to a level exceeding the threshold of the subsequent cascading, the wavevectors of the sideband and decay mode will be $\mathbf{k}_1' = \hat{\mathbf{z}}k_0 - \hat{\mathbf{x}}k_\perp$ and $\mathbf{k}_3' = (\hat{\mathbf{x}} + \hat{\mathbf{y}})k_\perp - \hat{\mathbf{z}}k_z$, which are separated from the $\mathbf{k}_1$ and $\mathbf{k}_3$ lines. This decay process continues when the $\mathbf{k}_1'$ line becomes strong enough to be a pump, which decays into a sideband with $\mathbf{k}_2' = \hat{\mathbf{z}}(k_0 + k_z') - \hat{\mathbf{y}}k_\perp$ and a decay mode with $\mathbf{k}_3'' = -(\hat{\mathbf{x}} - \hat{\mathbf{y}})k_\perp - \hat{\mathbf{z}}k_z'$; again $|k_z'/k_\perp| \ll 1$.

From (7), the coupled mode equation for the Langmuir sideband is obtained as

$$\{[(\partial_t + \nu_e)^2 + \Omega_e^2](\partial_t^2 + \nu_e\partial_t + \omega_p^2 - 3v_{te}^2\nabla^2)\nabla^2 - \Omega_e^2(\omega_p^2 - 3v_{ts}^2\nabla^2)\nabla_\perp^2\}\phi_2$$

$$= -\omega_p^2\left\{[(\partial_t + \nu_e)^2\boldsymbol{\nabla} + \Omega_e^2\boldsymbol{\nabla}_z]\cdot\left\langle\boldsymbol{\nabla}\phi_1\left(\frac{n_3^*}{n_0}\right)\right\rangle\right.$$

$$\left. -\boldsymbol{\Omega}_e(\partial_t + \nu_e)\hat{\mathbf{z}}\cdot\left\langle\boldsymbol{\nabla}\left(\frac{n_3^*}{n_0}\right)\times\boldsymbol{\nabla}\phi_1\right\rangle\right\}. \tag{36}$$

For the lower-hybrid decay mode $n_3(\omega_3, \mathbf{k}_3)$, $\Omega_i^2 \ll |\omega_3|^2 \ll \Omega_e^2$, and $|\partial_t^2\nabla_\perp^2|$ and $|\Omega_e^2\nabla_z^2|$ are of the same order of magnitude. Thus, the coupled mode equation (8) is reduced to

$$\partial_t\left\{\nabla_\perp^2(\partial_t + \nu_e)[\partial_t(\partial_t + \nu_i) - C_s^2\nabla^2] + \boldsymbol{\Omega}_e\boldsymbol{\Omega}_i\left(\nabla_\perp^2 + \frac{M\nabla_z^2}{m}\right)\partial_t\right\}\frac{n_3}{n_0}$$

$$= \frac{m}{M}\nabla^2\left[(\partial_t + \nu_e)\partial_t\boldsymbol{\nabla}_\perp\cdot\mathbf{a}_p + \Omega_e^2\partial_z a_{pz} - \frac{\Omega_e^2\partial_t\boldsymbol{\nabla}\cdot\mathbf{J}_B}{n_0 - \boldsymbol{\Omega}_e\partial_t\boldsymbol{\nabla}\cdot\mathbf{a}_p\times\hat{\mathbf{z}}}\right]. \tag{37}$$

https://doi.org/10.1017/S0022377801001477 Published online by Cambridge University Press

It is found that the third and fourth coupling terms on the right-hand side of (37) cancel each other. This leaves the first two terms on the right-hand side of (37), attributed to the transverse convective force and parallel ponderomotive force, as the dominant coupling terms.

Again, considering spatial and temporal harmonic perturbations having a general expression $p = \not{p}\exp[i(\boldsymbol{\kappa}\cdot\mathbf{r}) - \tilde{\omega}t)]$, where $\boldsymbol{\kappa}$ and $\tilde{\omega}$ are the appropriate wavevector and frequency of each perturbation, (36) and (37) can be combined to obtain the dispersion relation of the instability as

$$[i\omega_0(2\gamma+\nu_e) - \Delta\omega_l^2][-i\omega_{30}(2\gamma+\nu_3) - \Delta\omega_3^2]$$
$$= 2\xi^{-1}\frac{e^2}{mM\omega_p^2}\cos^2\theta\frac{1+i\Omega_e/\omega_0}{\omega_0^2-\Omega_e^2}\left(\frac{1+i\Omega_e\omega_0\tan^2\theta}{\omega_0^2-\Omega_e^2}\right)k_0^2k_\perp^2|\varphi_1|^2, \qquad (38)$$

where $\omega_3 = \omega_{30} + i\gamma$ is assumed and γ is the growth rate of the instability;

$$\Delta\omega_l^2 = 2\omega_0(N\omega_{30} + \tfrac{1}{2}\nu_e) + \Delta\omega_m^2 - \Delta\omega_{m0}^2$$

for the Nth cascade

$$\Delta\omega_3^2 = 2k_\perp^2C_s^2 + \Omega_e\Omega_i\xi + \nu_e\nu_i - \omega_{30}^2, \qquad \nu_3 = \nu_i + \nu_e\left(1 - \frac{2k_\perp^2C_s^2}{\omega_{30}^2}\right), \qquad \xi = 1 + \frac{Mk_z^2}{2mk_\perp^2},$$

and

$$\frac{\nu_e}{\omega_{30}} \ll \frac{\Omega_e}{\omega_0}, \qquad \frac{k_\perp^2\Omega_e^2}{k_1^2\omega_0^2} \ll 1$$

are assumed. Equation (38) leads to two real equations for determining the real frequency ω_{30} of the decay mode and the growth rate γ of the instability. We first determine the threshold field by setting $\gamma = 0$ in (38). The resulting equation is then solved to obtain

$$\omega_{30} \approx \left[2k_\perp^2C_s^2 + \Omega_e\Omega_i\xi - \frac{\xi\nu_3\omega_0\Omega_i}{(\cos^2\theta - \Omega_e^2/\omega_0^2)(2k_\perp^2C_s^2 + \Omega_e\Omega_i\xi)^{1/2}}\right]^{1/2} \qquad (39)$$

and

$$|\varphi_1|_{\text{th}}^2 = \left(\frac{m}{e}\right)^2\frac{\nu_e\Omega_e}{2\omega_{30}\omega_0}\frac{\xi(\omega_0^2-\Omega_e^2)^2\Delta\omega_l^2}{(\omega_0^2\cos^2\theta - \Omega_e^2)k_0^2k_\perp^2}. \qquad (40)$$

The growth rate is found to be

$$2\gamma = \left[\nu_e^2 + \left(\nu_e^2 + \frac{\Delta\omega_l^2\nu_e\Omega_i}{\omega_{30}^2}\right)\left(\frac{|\varphi_1|^2}{|\varphi_1|_{\text{th}}^2} - 1\right)\right]^{1/2} - \nu_e, \qquad (41)$$

where the slight frequency shift of the decay mode with the pump field is neglected.

Since the threshold field of (40) increases with $\Delta\omega_l$, and $\Delta\omega_l^2$ increases with the number of the cascading process, the cascading process eventually stops when the threshold field becomes too high. Using the ionospheric parameters of the Arecibo heating experiments given in the preceding section, (40) is expressed numerically as

$$|\mathscr{E}|_{\text{th}} = 0.636\xi^{1/2}[N + 3.22\xi^{-1/2}(\tan^2\theta - \tan^2\theta_0)$$
$$+17.86\xi^{-1/2}(\sin^2\theta - \sin^2\theta_0)]^{1/2}/\cos^2\theta\sin\theta \quad (\text{in V m}^{-1}). \qquad (42)$$

Therefore, the threshold field for the Nth cascade of $(k_1, 40^\circ)$ lines occurring near the

https://doi.org/10.1017/S0022377801001477 Published online by Cambridge University Press

HF wave reflection height in the layer at $h = h_0$, where $\omega_p^2(h_0) = \omega_0(\omega_0+\nu_e)-3k_0^2\nu_{te}^2$, i.e., $\theta_0 = 0$, is given by

$$|\mathscr{E}_1(h_0)|_{\rm th} = 1.69\xi^{1/2}(N + 9.65\xi^{-1/2})^{1/2} \qquad (\text{in V m}^{-1}) \tag{43}$$

and for those occurring in their matching height layer at $h = h_1$, where $\omega_p^2(h_1) = \omega_0(\omega_0 + \nu_e) - 3k_l^2v_{te}^2 - \Omega_e^2\sin^2 40°$, i.e., $\theta_0 = 40°$, it becomes

$$|\mathscr{E}_1(h_1)|_{\rm th} = 1.69\xi^{1/2}N^{1/2} \qquad (\text{in V m}^{-1}) \tag{44}$$

The threshold field (44) is smaller than that given by (43). Using the case $\xi = 1$ as an example, the OTSI threshold fields for exciting $(k_1, 40°)$ sidebands in the layers at $h = h_0$ and h_1 are $6.06\,\text{V m}^{-1}$ and $0.222\,\text{V m}^{-1}$, respectively. Since the threshold fields in (43) and (44) are proportional to $\xi^{1/4}$, the decay instability prefers to excite the field-aligned lower-hybrid resonance mode having $\xi = 1$.

We now examine the threshold conditions for producing broad frequency-downshifted HFPLs of 50 kHz bandwidth, as an example, in different altitude regions. It is noted that the lower-hybrid frequency is proportional to $\xi^{1/2}$; thus, a larger ξ will need fewer cascades to obtain the same bandwidth. However, the threshold field of each cascade, as shown by (43) and (44), increases with increasing ξ. It turns out that the pump threshold field for the overall process is minimum in the case of $\xi = 1$, which has $f_{30} \approx 6.2$ kHz. Thus, $N = 8$ is needed. The threshold field evaluated from (43) for the case $N = 8$ is $4.77\,\text{V m}^{-1}$. In general, Langmuir waves excited by the OTSI saturate at amplitudes about twice of that of the HF pump wave. Thus, the HF field amplitude required in order to reach $N = 8$ in the matching height layer of the HFPLs is estimated to be about $2.4\,\text{V m}^{-1}$. On the other hand, the threshold field required for producing the same broad downshifted HFPLs indirectly (involving scattering or filamentation instability) or directly in the layer at $h = h_0$ near the reflection height of the O-mode HF heating wave is $3.6\,\text{V m}^{-1}$ or $6.06\,\text{V m}^{-1}$, respectively. The cascades produce HFPLs of 50 kHz bandwidth, whose frequencies are downshifted continuously from the HF wave frequency.

However, it is also noted that, due to the swelling effect, the HF wave electric field amplitude increases with altitude in the region near the HF reflection height. The ratio of the heating wave field amplitudes at the two heights should be estimated in order to draw a proper conclusion about where the preferential altitude is. Without considering anomalous absorption, one can estimate the field amplitude ratio at the two heights by applying the continuity of HF energy fluxes in the upward and downward directions as follows: $E_1/H_1 = \eta_1$ and $E_2/H_2 = \eta_2$, where $\eta = (\mu/\epsilon)^{1/2}$ is the characteristic impedance of the medium (background plasma), and the subscripts 1 and 2 represent the locations at the reflection height and matching height, respectively.

Continuity of the energy flux of the HF heating wave, $E_1H_1 = E_2H_2$, leads to

$$\left(\frac{E_1}{E_2}\right)^4 = \frac{\epsilon_2}{\epsilon_1} = \frac{1-\omega_{p2}^2/\omega_0^2}{1-\omega_{p1}^2/\omega_0^2} = \frac{3k_1^2v_{te}^2 + \Omega_e^2\sin^2\theta_0 - \omega_0\nu_e}{3k_0^2v_{te}^2 - \omega_0\nu_e}. \tag{45}$$

Using the values of the parameters given in Sec. 2 yields $E_1/E_2 < 1.5$. Therefore, the

matching height of the HFPLs is shown to be the preferential altitude of exciting a broad downshifted spectrum of HFPLs in the Arecibo heating experiments.

7. Discussion

Cascades of Langmuir sidebands of the PDI and OTSI excited in the ionospheric heating experiments via two secondary parametric instability processes have been studied. One process cascades Langmuir waves through ion acoustic waves, the other through lower-hybrid waves.

In the first case, cascading through ion acoustic waves, both resonant and non-resonant cascading processes have been analyzed. In the resonant decay case, the propagation loss of Langmuir waves imposes a large power ratio $e^{2\alpha\Delta z}$ ($\approx 10\,\mathrm{dB}$) on the two consecutive cascade lines in the HFPLs. However, since such a large power ratio was not shown in experimental results, the cascade of the PDI is not likely to be through the resonant cascading process.

Through the nonresonant cascading processes, it is shown from (35) that the threshold power for exciting the Nth cascade line is proportional to N^2 in the parameter range where $2N\nu_i < \nu_e$ and $k^2C_s^2/\nu_e^2 \gg 1$. The threshold field of this secondary parametric instability as the cascading process is much higher than that of the PDI (as shown by (30)), and it increases with the square of the number N of cascade steps (as shown by (35)). Thus, the maximum number of cascade lines excited by an HF heating wave turns out to be much less than that determined by the condition: $2\,\mathrm{Int}(P_0/P_{\mathrm{th}} - 1) \leqslant N \leqslant 2\,\mathrm{Int}(P_0/P_{\mathrm{th}} - 1) + 1$ (Stubbe et al. 1992), where P_0 and P_{th} are the heating wave power and the threshold power of the PDI, respectively, and Int(...) denotes the integer part of (...). For example, the threshold power for the excitation of the third cascade line is about 3.5 dB higher than that for the excitation of the second cascade line. The experimental result shows that the saturation intensity of the second cascade line can be larger than that of the first cascade line, but the difference rarely exceeds 3.5 dB. This explains why the second cascade line hardly generates a third in Tromsø early heating experiments. In Arecibo, with $\nu_i \approx \nu_e$, the increase rate of the threshold field with the number of the cascade step ($\propto N^{1/2}$) is not as fast as that ($\propto N^2$) in Tromsø heating experiments. Consequently, more cascade steps can occur in the Arecibo heating experiments.

The second case of cascading through the lower-hybrid wave studies the feasibility of generating a broad spectrum of frequency-downshifted HFPLs in the same altitude region by O-mode HP heating waves in the Arecibo heating experiments. It is, however, noted that the theory is also applicable for heating experiments conducted at other heater sites. This process starts with the OTSI or PDI. It was first shown that the excitation of the OTSI is not restricted to the region near the reflection height of the O-mode HF heating wave. Owing to the geomagnetic field and smooth plasma density gradient in the F region of the ionosphere, the OTSI can be excited in a sizable spatial region below the HF reflection height. In fact, obliquely propagating Langmuir sidebands are preferentially excited in their matching heights by the OTSI (as well as by the PDI), where the altitudes move downward as their oblique propagation angles increase. Therefore, the OTSI and PDI generate Langmuir waves in a sizable altitude range. Once these Langmuir waves grow to large enough amplitudes, they decay into frequency-downshifted

https://doi.org/10.1017/S0022377801001477 Published online by Cambridge University Press

Langmuir sidebands and lower-hybrid waves. A conventional two-dimensional arrangement matching them on the plane of the pump wavevector and the geomagnetic field was first chosen, and it was found that the product of the coupling terms of the two-coupled mode equations has the wrong sign, i.e., there is no instability. This sign changes when the wavevectors of three waves are matched in three-dimensional space. In other words, this secondary parametric instability is a three-dimensional process. Continuous cascades of Langmuir sidebands through the same process lead to a broad spectrum of frequency-downshifted Langmuir waves.

Lower-hybrid waves, in general, have a broad and continuous spectrum. The frequency of the lower-hybrid wave increases with increasing parallel component of its wavevector. For a given bandwidth of the cascade spectrum, the required number of cascades decreases as the frequency of the lower-hybrid decay mode in the cascade process increases. However, the threshold field of the Langmuir pump wave in each cascade step also increases with increasing frequency of the lower-hybrid decay mode. The two effects counterbalance each other. It turns out that the cascading process having the field-aligned lower-hybrid resonance mode as the decay mode requires the minimum threshold field from the HF heating wave. But the HF threshold field for the overall process is, in fact, quite independent of the frequency of the lower-hybrid decay mode. Considering the field-aligned lower-hybrid resonance mode as the decay mode, the results of the analysis for the Arecibo heating experiments show that for the OTSI-excited Langmuir waves to be able to cascade eight times in the HF reflection height region, the HF wave field amplitude has to exceed $3.6\,\mathrm{V\,m^{-1}}$. Then the generated Langmuir waves will have a 50 kHz bandwidth below the HF wave frequency, but their propagation directions will be confined in a narrow cone ($< 30°$) around the geomagnetic field. Therefore, an additional process, such as the filamentation instability (Kuo et al. 1993) or scattering with the short-scale field-aligned density irregularities, is also involved to convert some of these Langmuir waves into HFPLs detected by the Arecibo UHF radar.

However, the threshold fields of the OTSI and PDI excited in matching height regions of their vertically propagating Langmuir sidebands are much lower than the corresponding fields required to generate vertically propagating Langmuir sidebands in the HF reflection height region. Thus, the HFPLs at the frequency of the HF heating wave and at the frequency downshifted from that of the HF heating wave by the ion acoustic frequency can be generated directly by the O-mode heating wave via the OTSI and PDI, respectively, in the respective matching height regions of the HFPLs. Hence, the cascade of 40° Langmuir sidebands excited directly by the O-mode heating wave via the OTSI and PDI in their matching height region were also analyzed for comparison. It was shown that the cascade of these 40° Langmuir sidebands can lead directly to a broad downshifted spectrum of HFPLs originating from the same altitude in the Arecibo heating experiments; however, this altitude is the matching height of the 40° Langmuir sidebands of the OTSI or PDI, rather than the reflection height of the O-mode heating wave. The threshold field of the heating wave is about $2.4\,\mathrm{V\,m^{-1}}$, which is less than the $3.6\,\mathrm{V\,m^{-1}}$ required for the same instabilities excited in the region near the HF reflection height. The swellling factor on the HF wave electric field amplitude increases with altitude in the region near the HF reflection height; however, the result of the analysis shows that the ratio of the swelling factors in the two regions is not large enough to make up the difference in threshold fields. It is also noted that the generated cascade spectrum is not in discrete form. This is because lower-hybrid waves have a

broad and continuous spectrum, which can be excited simultaneously as different frequency decay modes in the cascade process.

In summary, this work has shown the following.

1. The threshold power of the cascading process through the ion acoustic wave has an N^2 dependence for $\nu_e \gg 2N\nu_i$ and an $N^{1/2}$ dependence for $\nu_e \ll 2N\nu_i$. This explains why the second cascade line generates hardly a third in the early Tromsø heating experiments before the superheater was in operation and why more cascade steps can occur in the Arecibo heating experiments.

2. In a magnetized plasma, the OTSI can be excited in a wide layer extending from the HF reflection height to a distance below that altitude. In fact, it is preferentially excited near the matching height of its Langmuir sidebands, which moves downward as the oblique propagation angles of sidebands increase; this is contrary to the unmagnetized case, where the OTSI can only be excited in a narrow layer near the reflection height of the HF pump wave.

3. A three-dimensional parametric instability process is feasible to generate a broad downshifted spectrum of HFPLs in the HF heating experiments. The preferential originating altitude of such a spectrum of HFPLs in the Arecibo heating experiments is found to be the matching height of HFPLs rather than the HF wave reflection height.

Acknowledgements

This work was supported in part by the High Frequency Active Auroral Research Program (HAARP), AFRL at Hanscom AFB, MA and in part by Office of Naval Research Grant ONR-N00014-00-1-0938.

References

Carlson, H. C., Gordon, W. E. and Showen, R. L. 1972 *J. Geophys. Res.* 77, 1242.

Dysthe, K. B., Mjolhus, E., Pecseli, H. L. and Stenflo, L. 1984 *Plasma Phys. Contr. Fusion* 26, 443.

Fejer, J. A. 1979 *Rev. Geophys.* **17**, 135.

Fejer, J. A. and Kuo, Y. Y. 1973 *Phys. Fluids* **16**, 1490.

Hagfors, T., Kofman, W., Kopka, H., Stubbe, P. and Aijanen, T. 1983 *Radio Sci.* **18**, 861.

Huang, J. and Kuo, S. P. 1994 *J. Geophys. Res.* **99**, 2173.

Isham, B., Kofman, W., Hagfors, T., Nordling, J., Thide, B., LaHoz, C. and Stubbe, P. 1990 *Radio Sci.* **25**, 251.

Isham, B., Rietveld, M. T., Hagfors, T., LaHoz, C., Mishin, E., Kofman, W., Leyser, T. B. and Van Eyken, A. P. 1999 *Adv. Space Res.* **24**, 1003.

Istomin, Y. and Leyser, T. 1995 *Phys. Plasmas* **2**, 2084.

Kasymov, Zh. Zh., Naslund, E., Stardub, A. N. and Stenflo, L. 1985 *Physica Scripta* **31**, 201.

Kuo, S. P. 1996 *Phys. Plasmas* **3**, 3957.

Kuo, S. P. 1997 *Phys. Plasmas* **4**, 3194.

Kuo, S. P. and Huang, J. 1996 *Phys. Plasmas* **3**, 4697.

Kuo, S. P. and Lee, M. C. 1999 *Geophys. Res. Lett.* **26**, 3289.

Kuo, S. P., Cheo, B. R. and Lee, M. C. 1983 *J. Geophys. Res.* **88**, 417.

Kuo, S. P., Lee, M. C. and Djuth, F. T. 1987 *Geophys. Res. Lett.* **14**, 961.

Kuo, S. P., Ho, A. Y. and Lee, M. C. 1990 *Geophys. Res. Lett.* **17**, 2209.

Kuo, S. P., Huang, J. and Lee, M. C. 1993 *J. Geophys. Res.* **98**, 11 671.

Kuo, S. P., Lee, M. C. and Kossey, P. 1997 *Geophys. Res. Lett.* **24**, 2969.

Kuo, S. P., Koretzky, E. and Lee, M. C. 1998 *J. Geophys. Res.* **103**, 23 373.
Lee, M. C. and Kuo, S. P. 1983 *J. Plasma Phys.* **30**, 463.
Lee, M. C., Riddolls, R. J., Burke, W. J., Kuo, S. P. and Klien, E. M. C. 1998 *Geophys. Res. Lett.* **25**, 3067.
Lee, M. C., Klien, E. M. C., Burke, W. J., Zhang A. X., Riddolls, R. J., Kuo, S. P. and Isham, B. 1999 *Geophys. Res. Lett.* **26**, 37.
Leyser, T. B. 1991 *Geophys. Res. Lett.* **18**, 408.
Leyser, T. B. 1994 *Phys. Plasmas* **1**, 2003.
Leyser, T. B., Thide, B., Derblom, H., Hedberg, A., Lundborg, B., Stubbe, P. and Kopka, H. 1989 *Phys. Rev. Lett.* **63**, 1145.
Mishin, E., Hagfors, T. and Kofman, W. 1997 *J. Geophys. Res.* **102**, 27 265.
Perkins, F. W., Oberman, C. and Valeo, E. J. 1974 *J. Geophys. Res.* **79**, 1478.
Rietveld, M. T., Isham, B., Kohl, H., LaHoz, C. and Hagfors, T. 2000 *J. Geophys. Res.* **105**, 7429.
Showen, R. L. and Behnke, R. A. 1978 *J. Geophys. Res.* **83**, 207.
Showen, R. L. and Kim, D. M. 1978 *J. Geophys. Res.* **83**, 623.
Stenflo, L. 1985 *J. Geophys. Res.* **90**, 5355.
Stenflo, L. 1990 *Physica Scripta* **T30**, 166.
Stenflo, L. 1991 *J. Plasma Phys.* **45**, 355.
Stenflo, L. and Shukla, P. K. 1988 *J. Geophys. Res.* **93**, 4115.
Stubbe, P. 1996 *J. Atmos. Terr. Phys.* **58**, 349.
Stubbe, P. and Kopka, H. 1990 *Phys. Rev. Lett.* **65**, 183.
Stubbe, P, Kopka, H., Jones, T. B. and Robinson, T. 1982 *J. Geophys. Res.* **87**, 1151.
Stubbe, P., Kopka, H., Thide, B. and Derblom, H. 1984 *J. Geophys. Res.* **89**, 7523.
Stubbe, P., Kopka, H., Rietveld, M. T., Frey, A., Hoeg, P., Kohl, H., Nielsen, E. and Rose, G. 1985 *J. Atmos. Terr. Phys.* **47**, 1151.
Stubbe, P., Kohl, H. and Rietveld, M. T. 1992 *J. Geophys. Res.* **97**, 6285.
Stubbe, P., Stocker, A. J., Honary, F., Robinson, T. R. and Jones, T. B. 1994 *J. Geophys. Res.* **99**, 6233.
Thide, B., Kopka, H. and Stubbe, P. 1982 *Phys. Rev. Lett.* **49**, 1561.
Westman, A., Leyser, T. B., Wannberg, G. and Rietveld, M. T. 1995 *J. Geophys. Res.* **100**, 9717.
Zhou, H. L., Huang, J. and Kuo, S. P. 1994 *Phys. Plasmas* **1**, 3044.
Zakharov, V. E. 1972 *Sov. Phys. JETP* **35**, 908.
Zakharov, V. E., Pushkarev, A. N., Rubenchik, A. M., Sagdeev, R. Z. and Shvets, V. F. 1972 *Sov. Phys. JETP* **47**, 287.